

Quantum Oscillation from In-gap States and Non-Hermitian Landau Level Problem

Huitao Shen and Liang Fu

Department of Physics, Massachusetts Institute of Technology, Cambridge, Massachusetts 02139, USA

Motivated by recent experiments on Kondo insulators, we theoretically study quantum oscillations from disorder-induced in-gap states in small-gap insulators. By solving a non-Hermitian Landau level problem that incorporates the imaginary part of electron's self-energy, we show that the oscillation period is determined by the Fermi surface area in the absence of the hybridization gap, and derive an analytical formula for the oscillation amplitude as a function of the indirect band gap, scattering rates, and temperature. Over a wide parameter range, we find that the effective mass is controlled by scattering rates, while the Dingle factor is controlled by the indirect band gap. We also show the important effect of scattering rates in reshaping the quasiparticle dispersion in connection with angle-resolved photoemission measurements on heavy fermion materials.

Quasiparticles in interacting/disordered systems generally have a finite lifetime due to the presence of electron-electron, electron-phonon or electron-impurity scattering. The decay of quasiparticles is formally described by the imaginary part of electron's self-energy. In small-gap systems, the decay of a quasiparticle can alter its energy-momentum dispersion significantly, for example, transform two-dimensional Dirac points into "bulk Fermi arcs" [1, 2].

In this work, we study the effect of quasiparticle lifetime on the quantum oscillation in small-gap insulators. The oscillation of various physical quantities, such as the magnetic susceptibility (de Haas-van Alphen effect) and resistivity (Shubnikov-de Haas effect) with respect to the magnetic field is usually regarded as a key characteristics of metals with a Fermi surface [3]. The period of the oscillation is determined by the Fermi surface area, and the amplitude decay with the temperature is determined by electron's effective mass. Intriguingly, recent experiments found quantum oscillations in heavy fermion materials SmB_6 [4, 5] and YbB_{12} [6, 7], which are Kondo insulators with a small energy gap. The physical origin of these quantum oscillations in insulators is hotly debated [8–14].

Motivated by, but not limited to, these experiments on Kondo insulators, we theoretically study quantum oscillations from disorder-induced in-gap states in small-gap insulators. In a generic two-band model with a hybridization gap, disorder leads to finite quasiparticle lifetime and in-gap states. The spectrum and width of Landau levels in a magnetic field is calculated by solving a *non-Hermitian* Landau quantization problem that incorporates the imaginary part of electron's self-energy. The density of states inside the gap, which comes from the tails of broadened Landau levels, is found to exhibit oscillations periodic in $1/B$. The period is given by the Fermi surface in the absence of hybridization. An analytical formula is derived for the oscillation amplitude as a function of the indirect band gap, scattering rates and the temperature. For a wide range of (but not all) parameters, the temperature dependence of the quantum oscillation is qualitatively similar to Lifshitz-Kosevich (LK) theory of normal metals [3, 15]. A key difference, however, is that

the cyclotron mass in the LK factor is not the band mass, but depends on the scattering rate. Moreover, the oscillation amplitude at a fixed temperature, i.e., the Dingle factor, is controlled by the indirect band gap, when the scattering rate is small.

The peculiarity of quantum oscillation amplitude we found in small-gap insulators, where the scattering rate controls LK factor instead of Dingle factor, is quite the opposite to the case of normal metals, where the scattering rate controls Dingle factor instead of LK factor. This result is an important prediction of our theory. It contrasts clearly with quantum oscillations from thermal excitations in Landau levels above the hybridization gap [8, 10]. In that scenario, the oscillation amplitude exhibits thermal activation behavior and drops to zero, instead of saturates, in the zero temperature limit.

We start by considering a generic two-band model with a hybridization gap:

$$H_0(\mathbf{k}) = \begin{pmatrix} \epsilon_1(k) & \Delta(\mathbf{k}) \\ \Delta(\mathbf{k}) & -\epsilon_2(k) \end{pmatrix}, \quad (1)$$

with $k \equiv |\mathbf{k}|$. Here the diagonal terms $\epsilon_1(k)$ and $-\epsilon_2(k)$ describe the dispersion of an electron-type and a hole-type band respectively, and $\Delta(\mathbf{k})$ describes their hybridization. The Hamiltonian H_0 in the inverted regime is widely used as a minimum model for the electronic structure of Kondo insulators at low temperature [16]. In this context, the two bands come from d - and f -orbitals, and exhibit an avoided crossing on a circle or a sphere in k space $|\mathbf{k}| = k_F$, which is set by the condition $\epsilon_1(k_F) + \epsilon_2(k_F) = 0$. Note that the hybridization gap $\delta(k_F) \equiv |\Delta(k_F)|$ is (much) larger than the indirect band gap δ , when the two bands are (highly) asymmetric, as shown in Fig. 1.

Disorder introduces in-gap states in the above model. The disordered Hamiltonian we shall study is $H = \sum_{\mathbf{k}} c_{\mathbf{k}}^\dagger H_0(\mathbf{k}) c_{\mathbf{k}} + \int d\mathbf{r} U(\mathbf{r}) c_{\mathbf{r}}^\dagger \Lambda c_{\mathbf{r}}$, where $c^\dagger \equiv (d^\dagger, f^\dagger)$ is the electron creation operator for the two orbitals. $U(\mathbf{r})$ is the impurity potential, which is assumed to be short-ranged and characterized by $\langle U(\mathbf{r})U(\mathbf{r}') \rangle = U_0 \delta(\mathbf{r} - \mathbf{r}')$ under disorder average $\langle \dots \rangle$. The electron-impurity scattering is allowed to be orbital dependent, so the scattering vertex takes the form $\Lambda = \alpha I + \beta \sigma_z$. In heavy fermion

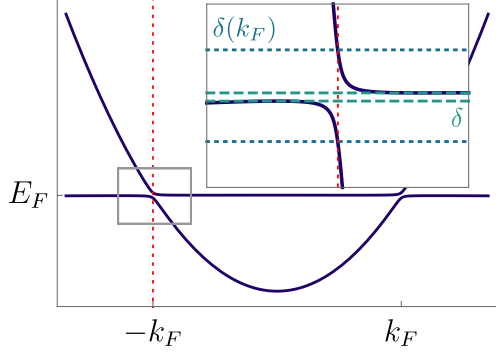


FIG. 1. Schematic band structure of a Kondo insulator. Inset: Zoom of the hybridization gap near $k = k_F$. $\delta(k_F)$ is the hybridization gap defined as the energy difference of the two bands at $k = k_F$. δ is the indirect band gap. Note in general $\delta < \delta(k_F)$.

systems, f -orbitals are tightly bound to the nucleus and thus scatter much less with impurities than d -orbitals do.

Using self-consistent Born approximation, we compute disorder-induced electron self-energy operator $\Sigma(\omega)$, which is a 2×2 matrix. In systems with p -wave hybridization, the self-energy is guaranteed by symmetry to be diagonal [17]. The real part of $\Sigma(\omega)$ renormalizes the chemical potential and the inverted gap at $k = 0$, and for convenience, will be absorbed into H_0 in the following. The imaginary part of the self-energy becomes a nonzero diagonal matrix when the disorder strength U_0 exceeds a critical value on the order of hybridization gap $\delta(k_F)$. At low energy $|\omega| \lesssim \delta(k_F)$, $\text{Im } \Sigma(\omega)$ is weakly dependent on ω , hence can be approximated by

$$\Sigma(\omega) \simeq \begin{pmatrix} -i\Gamma_1 & 0 \\ 0 & -i\Gamma_2 \end{pmatrix} \equiv -i(\Gamma I + \gamma \sigma_z)/2. \quad (2)$$

Here $\Gamma_1, \Gamma_2 > 0$ are the inverse lifetimes of quasiparticles on the d - and f -band respectively, and we have defined $\Gamma \equiv \Gamma_1 + \Gamma_2$ and $\gamma \equiv \Gamma_1 - \Gamma_2$. Generally, $\Gamma_1 \neq \Gamma_2$ or $\gamma \neq 0$, as the two bands have different masses and disorder potentials.

The imaginary part of electron's self-energy modifies and broadens the quasiparticle dispersion, and creates in-gap states. To see this, we compute the spectral function $A(\mathbf{k}, \omega) = -2\text{Im} [1/(w - H_0(\mathbf{k}) - \Sigma)]$. For a given \mathbf{k} , $A(\mathbf{k}, \omega)$ is a sum of Lorentzians associated with the poles of the Green's function $\mathcal{E}_{\pm}(\mathbf{k})$, which are complex eigenvalues of the non-Hermitian quasiparticle Hamiltonian $H(\mathbf{k}) \equiv H_0(\mathbf{k}) + \Sigma$. For our two-band model and self-energy defined by Eq. (1) and (2), the two eigenvalues $\mathcal{E}_{\pm}(\mathbf{k})$ are given by [1]

$$\mathcal{E}_{\pm}(\mathbf{k}) = \frac{1}{2} \left(\epsilon_1(k) - \epsilon_2(k) - i\Gamma \pm \sqrt{(\epsilon_1(k) + \epsilon_2(k) - i\gamma)^2 + \Delta^2(\mathbf{k})} \right) \quad (3)$$

The real part of $\mathcal{E}_{\pm}(\mathbf{k})$, denoted as $\epsilon_{\pm}(\mathbf{k})$, is the dispersion of quasiparticle conduction and valence band, while

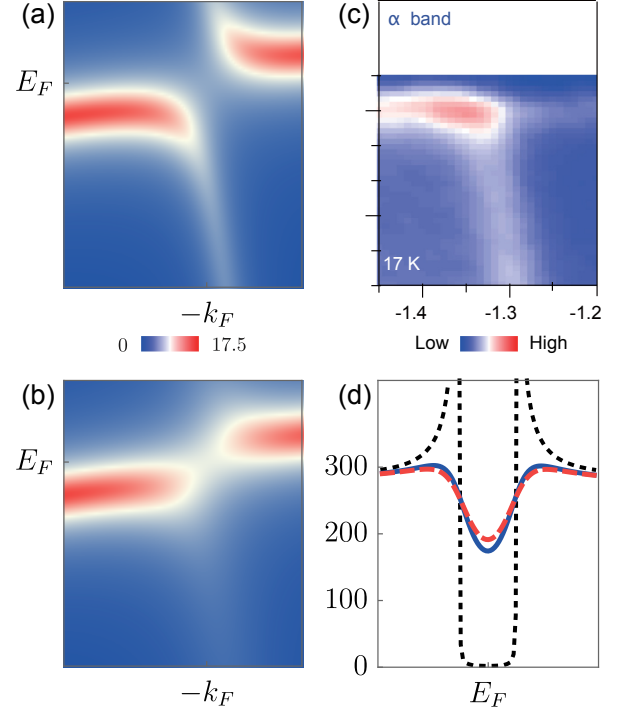


FIG. 2. (a) Spectral function $A(\mathbf{k}, \omega)$ for model $\epsilon_i = k^2/(2m_i) - \mu_i$ ($i = 1, 2$), where $m_2/m_1 = 50$, $\delta(k_F)/(\mu_2 - \mu_1) = 0.01$, $\Gamma_2/\delta(k_F) = 0.1$, $\Gamma_1/\delta(k_F) = 0.7$. The unit for colorbar is $1/\delta(k_F)$. (b) Same as (a) but with $\Gamma_1/\delta(k_F) = 1.7$. (c) ARPES data of CeCoIn₅ taken from FIG. 6 in Ref. [18]. (d) Momentum integrated spectral function $A(\omega)$ for model in (a) (blue, solid) and (b) (red, dashed) and in the clean limit $\Gamma_1 = \Gamma_2 = 0$ (black, dotted). The unit for $A(\omega)$ is $\sqrt{m_1 m_2}$.

its imaginary part determines the width of the broadened spectral function. In the special case of a single scattering rate $\Gamma_1 = \Gamma_2$ or $\gamma = 0$, the imaginary part is a constant so that the original band dispersion of $H_0(\mathbf{k})$ is broadened uniformly.

In the general case of two distinct scattering rates $\Gamma_1 \neq \Gamma_2$, however, $H_0(\mathbf{k})$ and Σ do not commute. Then $\gamma \neq 0$ has the nontrivial effect of altering the quasiparticle band dispersion $\epsilon_{\pm}(\mathbf{k})$, namely, damping reshapes dispersion. In particular, the quasiparticle hybridization gap at $k = k_F$ becomes reduced, given by

$$\epsilon_+(k_F) - \epsilon_-(k_F) = \begin{cases} \sqrt{\delta^2(k_F) - \gamma^2}, & \text{when } |\gamma| < \delta(k_F), \\ 0, & \text{when } |\gamma| \geq \delta(k_F). \end{cases} \quad (4)$$

With increasing disorder, the scattering rates $\Gamma_{1,2}$ and hence $|\gamma|$ increases. Above a critical amount of disorder $|\gamma| > \delta(k_F)$, the quasiparticle gap completely vanishes, leading to a disorder-induced semimetal. In the semimetallic phase, the quasiparticle conduction and valence bands stick together on the Fermi surface $|\mathbf{k}| = k_F$, despite that the hybridization term is present. Such band sticking without fine tuning is a remarkable and topologically robust feature which is unique to non-Hermitian band theory of finite-lifetime quasiparticles [19], but for-

bidden by level repulsion in Hermitian band theory. As we shall show later, quantum oscillation appears in both insulator and semimetal phases.

In Fig. 2, we plot the momentum-resolved spectral function $A(\mathbf{k}, \omega)$ and the momentum-integrated density of states $A(\omega) \equiv \int d\mathbf{k} A(\mathbf{k}, \omega)$ for different choices of scattering rates $\Gamma_{1,2}$. Due to its localized nature, the f -orbital has a smaller disorder-induced scattering rate $\Gamma_2 < \Gamma_1$. Panel (a) and (b) correspond to $|\gamma| < \delta(k_F)$ and $|\gamma| > \delta(k_F)$ respectively. Despite the simplicity of our model, the spectral function in panel (a) compares well with recent high-resolution angle-resolved photoemission spectroscopy (ARPES) data on the heavy fermion material CeInCo₅ taken at low temperatures [18]. We emphasize that the presence of two distinct scattering rates is necessary to reproduce many important features of the ARPES data, which cannot be captured using $\Gamma_1 = \Gamma_2$ [17]. We also note a systematic temperature-dependent ARPES study of the Kondo insulator SmB₆ showing that f -state spectra peak grows in height and narrows at low temperatures [20]. This observation is consistent with the existence of well-defined electron quasiparticles in the zero temperature limit, but does not favor the scenario of fractional excitations.

Due to the disorder scattering, the hybridization gap is partially filled, as shown by the density of states $A(\omega)$ in Fig. 2(d). Assuming the hybridization gap and scattering rates are small compared to the d -state band width, the density of states at low energy can be computed analytically [17]

$$A(\omega) = D_0 \text{Im} \left[\frac{1}{\sqrt{\delta^2/(\omega + i\Gamma_A)^2 - 1}} \right]. \quad (5)$$

with

$$\Gamma_A = \frac{m_1\Gamma_1 + m_2\Gamma_2}{m_1 + m_2}, \quad \delta \equiv \frac{\sqrt{m_1m_2}}{m_1 + m_2} \delta(k_F). \quad (6)$$

Here $D_0 = D_1 + D_2$ is the total density of states from both the d - and f -bands at the Fermi energy $\omega = 0$ in the absence of hybridization gap, and δ is the indirect band gap in the clean limit. The imaginary part Γ_A , a weighted sum of the two scattering rates, leads to disorder-induced broadening of density of states. Since the f band has a much larger mass $m_2 \gg m_1$, the indirect gap δ is much smaller than the hybridization $\delta(k_F)$, and even a small scattering rate Γ_2 is sufficient to generate considerable density of states within the gap. We note that in-gap states were found in SmB₆ by numerous experiments, see e.g. Ref. [21, 22], although its origin remains an open question.

We now show that in-gap density of states in our model exhibits quantum oscillation under a quantizing magnetic field. To the leading order approximation, the scattering rates are taken to be field independent. The density of states for $B \neq 0$ is then given by $A(\omega) = -(B/\pi) \text{Im} \sum_j [1/(\omega - \mathcal{E}_j)]$, where \mathcal{E}_j denotes the complete set of complex eigenvalues of the non-Hermitian

Hamiltonian with Pierels substitution $\mathbf{k} \rightarrow \mathbf{k} - \mathbf{A}$, i.e., $H(B) = H_0(\mathbf{k} - \mathbf{A}) + \Sigma$ (we set $e = \hbar = 1$).

For concreteness, we consider two bands in Eq. (1) with quadratic dispersion in two dimensions: $\epsilon_i = k^2/(2m_i) - \mu_i$ ($i = 1, 2$), where $m_{1,2} > 0$ are the effective masses for d - and f -bands respectively. We take an isotropic p -wave hybridization gap: $\Delta(\mathbf{k}) = v(k_x s_x + k_y s_y)$. Its band structure is schematically shown in Fig. 1.

The exact non-Hermitian Landau level spectrum of $H(B)$ is derived analytically [17]. Each Landau level $n \geq 1$ consists of two sets of complex eigenvalues in each spin sector denoted by $s = \uparrow, \downarrow$:

$$\mathcal{E}_{n \geq 1, \pm}^s = \frac{1}{2} \left(\epsilon_{1,n}^s - \epsilon_{2,n}^s - i\Gamma \right. \\ \left. \pm \sqrt{[(\epsilon_{1,n}^s + \epsilon_{2,n}^s) - i\gamma]^2 + v^2(8nB)} \right), \quad (7)$$

where $\epsilon_{1,n}^s = B(n \pm 1/2)/m_1 + \mu_1$ and $\epsilon_{2,n}^s = B(n \mp 1/2)/m_2 + \mu_2$ (with upper/lower sign for $s = \uparrow, \downarrow$). For high Landau level $n \gg 1$, the exact result Eq. (7) is identical to the one obtained by simply replacing $k \rightarrow \sqrt{2nB}$ in the zero-field dispersion (Eq. (3)), and is thus also identical for both spin sectors. This agreement shows that semi-classical approximation remains valid for Landau quantization of finite-lifetime quasiparticles whose self-energy has an imaginary part.

Typical Landau level energy spectrum, or the real part of $\mathcal{E}_{n,\pm}^s$ is plotted as a function of the magnetic field in Fig. 3(a) for the insulator phase, and (b) for the disorder-induced metal phase. Band edge oscillation can be seen clearly in both cases. For a given Landau level n , the hybridization gap is minimized when $B = k_F^2/(2n)$. In this way, the band edges of Landau levels oscillate with period $\Delta(1/B) = 2/k_F^2 = 2\pi/S_F$, where $S_F \equiv \pi k_F^2$ is the Fermi surface area in the absence of the hybridization. The oscillation of Landau level band edges leads to the oscillation of spectral function inside the gap, as the spectral weights inside the gap come from the tail of the broadened Landau levels. This effect, originated from the lifetime effect, persists even at zero temperature and in the limit of small (but nonzero) scattering rates.

We now calculate quantitatively the field- and temperature-dependent density of states inside the gap, defined as $D(\omega, T) \equiv -\int_{-\infty}^{+\infty} dE \frac{\partial n_F(E - \omega, T)}{\partial E} A(E)$, where $n_F(\mu, T) = (e^{(E-\mu)/T} + 1)^{-1}$ is the Fermi-Dirac distribution function. Under the assumption of small hybridization gap $\delta(k_F) \ll k_F^2/\sqrt{m_1m_2}$, weak magnetic field $B \ll k_F^2$ and low temperature $T \ll \delta(k_F), B/m_{1,2}$, the density of states can be analytically computed as [17]

$$D(\omega = 0, T) = \\ -4 \cos \left(\frac{\pi k_F^2}{B} \right) \sum_{i=\pm} \frac{M_i \frac{\pi^2 T}{\omega_{c,i}}}{\sinh \left(\frac{2\pi^2 T}{\omega_{c,i}} \right)} \exp(-\pi \mathcal{D}_i), \quad (8)$$

where $\omega_{c,i} \equiv B/M_i$ are the cyclotron frequencies associ-

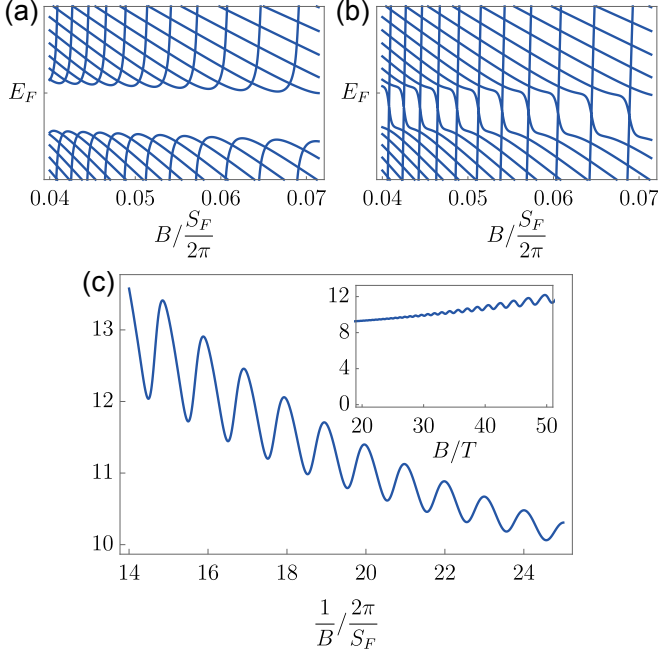


FIG. 3. (a) Real part of the Landau level spectrum $\text{Re}[\mathcal{E}_{n,\pm}^\downarrow]$ as function of magnetic field, whose model parameter is the same as that in Fig. 2(a). The spectrum for $s=\uparrow$ sector is similar. (b) Same as (a) but with model the same as that in Fig. 2(b). (c) Exact numerics of spectral function $A(\omega = 0)$ as function of $1/B$ and B (inset). The unit for $A(\omega)$ is $\sqrt{m_1 m_2}$. The model is the same as that in Fig. 2(a), with $m_1 = m_e$ being the free electron mass, hybridization gap being $\delta(k_F) = 1\text{meV}$. The resulting oscillation frequency is $F = 891\text{T}$.

ated with the following effective masses

$$M_\pm = \frac{(m_1 + m_2)}{2} \left[\frac{1}{\sqrt{1 + \delta^2/\Gamma_A^2}} \pm \frac{m_1 - m_2}{m_1 + m_2} \right], \quad (9)$$

and \mathcal{D}_\pm are the renormalized Dingle exponents

$$\mathcal{D}_\pm = \frac{1}{B/(m_1 + m_2)} \left(\Gamma_A \sqrt{1 + \delta^2/\Gamma_A^2} \pm \Gamma_D \right), \quad (10)$$

where $\Gamma_D \equiv (m_1 \Gamma_1 - m_2 \Gamma_2)/(m_1 + m_2)$.

The analytical formula for the quantum oscillation amplitude, Eq. (8), is one of our main results. It is a sum of two oscillating components that share the same period $\Delta(1/B) = 2\pi/S_F$. This periodicity is consistent with our expectation from the Landau level spectrum shown in Fig. 3, and has also been reported in previous works without including lifetime effects [8, 10, 13]. Note that this result is not completely obvious, as the conduction band minimum and valence band maximum are located at two different momenta $k_\pm \equiv \sqrt{k_F^2 \pm (m_1 - m_2)\delta}$, rather than at k_F [17]. Instead of having two periods given by k_\pm^2 , the oscillation has a single period given by k_F^2 , the Fermi surface area of the two bands in the absence of hybridization.

The oscillation amplitude in Eq. (8) is determined by two scattering rates Γ_A and Γ_D , the indirect band gap δ

and the temperature T . It reduces to familiar results in various limits. In the gapless limit $\delta(k_F) = 0$, we reproduce the LK factors and Dingle factors for two metals. In the clean limit $\Gamma_1 = \Gamma_2 = 0$, there is no density of state within the gap to the leading order of temperature and we find $D(\omega = 0, T) = 0$.

Although Eq. (8) is valid both in the insulating phase $\Gamma_{1,2} \ll \delta(k_F)$ and in the semimetallic phase $|\gamma| > \delta(k_F)$, in the following we focus on the insulating phase, which applies to Kondo insulators. A detailed study of the disorder-induced semimetallic phase will be presented elsewhere.

We first analyze the simplest particle-hole symmetric model when $m_1 = m_2 = m$ and $\Gamma_1 = \Gamma_2 = \Gamma$. In this case, $\Gamma_A = \Gamma$, $\Gamma_D = 0$, and the LK effective mass and the Dingle exponent are

$$M = \frac{m}{\sqrt{1 + \delta^2/\Gamma^2}}, \quad \mathcal{D} = \frac{\sqrt{\Gamma^2 + \delta^2}}{B/(2m)}. \quad (11)$$

For small scattering rate $\Gamma \ll \delta$, they reduce to $M \sim m\Gamma/\delta$ and $\mathcal{D} \sim \delta/(B/2m)$. Decreasing the damping rate Γ leads to a smaller LK effective mass, and the Dingle exponent remains a constant controlled by the band gap.

The LK effective mass reflects the density of states inside the gap, since finite temperature effect is a thermal sampling of the spectral function through the convolution. Therefore, it is not a coincidence that Eq. (5) and Eq. (9) look similar. Indeed, the zero field density of states inside the gap is $A(\omega = 0) \sim m\Gamma/\delta = M$, which is exactly the LK effective mass.

In the more general setting of asymmetric model $m_1 \neq m_2$ and $\Gamma_1 \neq \Gamma_2 \ll \delta(k_F)$, the LK effective mass can vary in a wide range between m_1 and m_2 with proper choices of δ and Γ_A . The Dingle exponent remains a constant controlled by the band gap. This is opposite to that in normal metals when the scattering rate does not affect the LK effective mass but the Dingle factor.

As a concrete example, we present the quantum oscillation of the same model in Fig. 2(a), whose spectral function resembles the ARPES data. The density of states as function of $1/B$ is shown in Fig. 3(c). Since $\Gamma_D \neq 0$, the oscillation component associated with the larger Dingle factor becomes dominant [23], whose LK effective mass is $M = 8.5m_e$, in between m_1 and m_2 .

We note that the band edge oscillation in the absence of the scattering rate is reported in Ref. [10]. Contrary to our theory, in that case, the quantum oscillation comes from thermally excited occupation of Landau levels above the gap, hence the oscillation amplitude vanishes at zero temperature. Similar LK behavior of quantum oscillation in an insulator is also reported in a recent numerical study [13], which is consistent with our result.

Both the LK effective mass and the Dingle factor provide testable predictions of our theory. The parameters in our analysis—the two scattering rates—can in principle be extracted from other measurements on in-gap density of states and ARPES spectral function, as shown

in Fig. 2. The oscillation of density of states inside the gap naturally leads to magnetic susceptibility oscillation, i.e., de Haas-van Alphen effect. It also contributes to the quantum oscillation in resistivity, and we leave a detailed study for future work. We hope the results of this work can help understand quantum oscillations in Kondo insulators, and perhaps equally as important, motivate further study of quantum oscillations from in-gap states in small-gap insulators in general.

ACKNOWLEDGMENTS

We thank Patrick Lee for insightful discussions and suggestions, Michal Papaj for collaboration on a related project, Lu Li and Yuji Matsuda for sharing their unpublished experimental results, and T. Senthil for interesting remarks. This work is supported by DOE Office of Basic Energy Sciences, Division of Materials Sciences and Engineering under Award DE-SC0010526. LF is partly supported by the David and Lucile Packard Foundation.

[1] Vladyslav Kozii and Liang Fu, “Non-Hermitian Topological Theory of Finite-Lifetime Quasiparticles: Prediction of Bulk Fermi Arc Due to Exceptional Point,” arXiv:1708.05841.

[2] Michal Papaj, Hiroki Isobe, and Liang Fu, “Bulk Fermi arc of disordered Dirac fermions in two dimensions,” arXiv:1802.00443.

[3] D. Shoenberg, *Magnetic Oscillations in Metals*, Cambridge Monographs on Physics (Cambridge University Press, 1984).

[4] G. Li, Z. Xiang, F. Yu, T. Asaba, B. Lawson, P. Cai, C. Tinsman, A. Berkley, S. Wolgast, Y. S. Eo, Dae-Jeong Kim, C. Kurdak, J. W. Allen, K. Sun, X. H. Chen, Y. Y. Wang, Z. Fisk, and Lu Li, “Two-dimensional Fermi surfaces in Kondo insulator SmB_6 ,” *Science* **346**, 1208–1212 (2014).

[5] B. S. Tan, Y.-T. Hsu, B. Zeng, M. Ciomaga Hatnean, N. Harrison, Z. Zhu, M. Hartstein, M. Kiourlappou, A. Srivastava, M. D. Johannes, T. P. Murphy, J.-H. Park, L. Balicas, G. G. Lonzarich, G. Balakrishnan, and Suchitra E. Sebastian, “Unconventional Fermi surface in an insulating state,” *Science* **349**, 287–290 (2015).

[6] Z. Xiang, Y. Kasahara, B. Lawson, T. Asaba, C. Tinsman, Lu Chen, K. Sugimoto, H. Kawaguchi, Y. Sato, G. Li, S. Yao, Y.L. Chen, F. Iga, Y. Matsuda, and Lu Li, “Quantum Oscillations of Electrical Resistivity in an Insulator,” under review.

[7] Hsu Liu, Mate Hartstein, Greg Wallace, Alexander John Davies, Monica Ciomaga Hatnean, Michelle D Johannes, Natalya Shitsevalova, Geetha Balakrishnan, and Suchitra E Sebastian, “Fermi surfaces in Kondo insulators,” *Journal of Physics: Condensed Matter* (2018).

[8] Johannes Knolle and Nigel R. Cooper, “Quantum Oscillations without a Fermi Surface and the Anomalous de Haas-van Alphen Effect,” *Phys. Rev. Lett.* **115**, 146401 (2015).

[9] Johannes Knolle and Nigel R. Cooper, “Excitons in topological Kondo insulators: Theory of thermodynamic and transport anomalies in SmB_6 ,” *Phys. Rev. Lett.* **118**, 096604 (2017).

[10] Long Zhang, Xue-Yang Song, and Fa Wang, “Quantum Oscillation in Narrow-Gap Topological Insulators,” *Phys. Rev. Lett.* **116**, 046404 (2016).

[11] G. Baskaran, “Majorana Fermi Sea in Insulating SmB_6 : A proposal and a Theory of Quantum Oscillations in Kondo Insulators,” arXiv:1507.03477.

[12] Onur Erten, Po-Yao Chang, Piers Coleman, and Alexei M. Tsvelik, “Skyrme Insulators: Insulators at the Brink of Superconductivity,” *Phys. Rev. Lett.* **119**, 057603 (2017).

[13] Simonas Grubinskas and Lars Fritz, “Modification of the Lifshitz-Kosevich formula for anomalous quantum oscillations in inverted insulators,” arXiv:1704.06403.

[14] Inti Sodemann, Debanjan Chowdhury, and T. Senthil, “Quantum oscillations in insulators with neutral Fermi surfaces,” arXiv:1708.06354.

[15] I. M. Lifshitz and A. M. Kosevich, “Theory of Magnetic Susceptibility in Metals at Low Temperature,” *Sov. Phys. JETP* **2**, 636–645 (1956).

[16] Alexander Cyril Hewson, *The Kondo Problem to Heavy Fermions*, Cambridge Studies in Magnetism (Cambridge University Press, 1993).

[17] See Supplemental Material for calculation details and supplemental discussions.

[18] Q. Y. Chen, D. F. Xu, X. H. Niu, J. Jiang, R. Peng, H. C. Xu, C. H. P. Wen, Z. F. Ding, K. Huang, L. Shu, Y. J. Zhang, H. Lee, V. N. Strocov, M. Shi, F. Bisti, T. Schmitt, Y. B. Huang, P. Dudin, X. C. Lai, S. Kirchner, H. Q. Yuan, and D. L. Feng, “Direct observation of how the heavy-fermion state develops in CeCoIn_5 ,” *Phys. Rev. B* **96**, 045107 (2017).

[19] Huitao Shen, Bo Zhen, and Liang Fu, “Topological Band Theory for Non-Hermitian Hamiltonians,” arXiv:1706.07435.

[20] Jonathan D Denlinger, James W Allen, Jeong-Soo Kang, Kai Sun, Byung-II Min, Dae-Jeong Kim, and Zachary Fisk, “ SmB_6 Photoemission: Past and Present,” in *Proceedings of the International Conference on Strongly Correlated Electron Systems (SCES2013)*, JPS Conference Proceedings, Vol. 3 (Journal of the Physical Society of Japan, 2014).

[21] N. J. Laurita, C. M. Morris, S. M. Koohpayeh, P. F. S. Rosa, W. A. Phelan, Z. Fisk, T. M. McQueen, and N. P. Armitage, “Anomalous three-dimensional bulk ac conduction within the Kondo gap of SmB_6 single crystals,” *Phys. Rev. B* **94**, 165154 (2016).

[22] N. Wakeham, P. F. S. Rosa, Y. Q. Wang, M. Kang, Z. Fisk, F. Ronning, and J. D. Thompson, “Low-temperature conducting state in two candidate topological Kondo insulators: SmB_6 and $\text{Ce}_3\text{Bi}_4\text{Pt}_3$,” *Phys. Rev. B* **94**, 035127 (2016).

[23] On the other hand, in the limit when Γ_D is very small, both LK effective masses are measurable. One may observe two plateaus in the amplitude temperature dependence as found in Ref.[10].

Supplemental Material for “Quantum Oscillation from In-gap States and Non-Hermitian Landau Level Problem”

Huitao Shen¹ and Liang Fu¹

¹*Department of Physics, Massachusetts Institute of Technology, Cambridge, Massachusetts 02139, USA*

CONTENTS

I. Model	2
A. Model Hamiltonian	2
B. Hybridzation Gap and Band Gap	2
II. Self-Consistent Born Approximation	2
A. Conditions for Diagonal Self-energy	3
B. Numerical Solutions	3
III. Momentum Resolved Spectral Function at Zero Field	4
IV. Low Energy Density of States at Zero Field	6
V. Low Energy Density of States under Magnetic Field	7
A. Landau Level Spectrum	7
B. Low Energy Density of States	8
References	10

In this Supplemental Material, we present calculation details and supplement discussions. Although we will focus on a special case of the generic two-band model (Eq. (1) in the main text), many conclusions are governed only by the low energy behavior of the model and are thus general.

I. MODEL

A. Model Hamiltonian

Consider the two-band model

$$H_0(\mathbf{k}) = \begin{pmatrix} \epsilon_1(k) & \Delta(\mathbf{k}) \\ \Delta(\mathbf{k}) & -\epsilon_2(k) \end{pmatrix}, \quad (1)$$

where the diagonal term is given by two quadratic bands in two dimensions

$$\epsilon_1 = \frac{k^2}{2m_1} + \frac{g}{2} + \mu_0, \quad \epsilon_2 = \frac{k^2}{2m_2} + \frac{g}{2} - \mu_0. \quad (2)$$

Here $k \equiv \sqrt{k_x^2 + k_y^2}$, $m_i > 0$ for $i = 1, 2$ are the effective masses for the two bands, g is the fundamental gap of the two bands at $k = 0$, and μ_0 is the constant energy shift for later convenience. $g < 0$ represents the inverted band regime, which is of our interest in this paper. For convenience, we define $1/m_{\pm} \equiv 1/m_1 \pm 1/m_2$. Without hybridization $\Delta(\mathbf{k}) = 0$, the two bands touch at $k_F \equiv \sqrt{-2m_+g}$. $\mu_0 \equiv -k_F^2/(4m_-)$ so that $\epsilon_1(k_F) = \epsilon_2(k_F) = 0$.

As in the main text, we take an isotropic p -wave hybridization gap: $\Delta(\mathbf{k}) = v(k_x s_x + k_y s_y)$. This Hamiltonian commutes with $\sigma_z s_z$ and hence is a sum of two Blocks: $H_0 = H^{\uparrow} \oplus H^{\downarrow}$, where $H^{\uparrow, \downarrow}$ is 2×2 matrix associated with spin sector $\sigma_z s_z = \pm 1$, whose off-diagonal element is $v(k_x \pm ik_y)$ respectively. Since $H^{\uparrow} = (H^{\downarrow})^T$, all the results for H^{\downarrow} can be easily transferred to H^{\uparrow} . In the following, we will only consider H^{\downarrow} , which can be seen as a 2×2 Hamiltonian with $\Delta(\mathbf{k}) = v(k_x - ik_y)$.

B. Hybridzation Gap and Band Gap

Before proceeding further, we would like to remark on the “gaps” involved in this model. The band dispersion of the Bloch Hamiltonian given by Eq. (1) and (2) is

$$E_{\pm}(k) = \frac{1}{2} \left[\frac{k^2 - k_F^2}{2m_-} \pm \sqrt{\left(\frac{k^2 - k_F^2}{2m_+} \right)^2 + \left(\frac{k\delta(k_F)}{k_F} \right)^2} \right], \quad (3)$$

where $\delta(k_F) \equiv 2\sqrt{-2m_+v^2g}$ is the energy difference of the two bands at $k = k_F$. $\delta(k_F)$ is also understood as the “hybridization gap”. However, in the general case when $m_1 \neq m_2$, the band gap is in fact indirect. By finding the solution of $\partial E_{\pm}/\partial k = 0$, the conduction band bottom and the valence band top are located at

$$k_{\pm}^2 = k_F^2 \pm \delta(k_F) \sqrt{m_1 m_2} \frac{m_1 - m_2}{m_1 + m_2}. \quad (4)$$

Here we assume $\delta(k_F) \ll k_F^2/m_+$ and take $m_1 < m_2$ without loss of generality. The indirect band gap is then

$$\delta \equiv E_+(k_+) - E_-(k_-) = \frac{\sqrt{m_1 m_2}}{m_1 + m_2} \delta(k_F). \quad (5)$$

In this way, Equation (4) can also be expressed with the indirect band gap: $k_{\pm}^2 = k_F^2 \pm (m_1 - m_2)\delta$.

When $m_2/m_1 = 50$, we have $\delta/\delta(k_F) = 0.14$. This is nearly 7 times difference. A schematic of the hybridization gap and the indirect band gap is shown in Fig. 1 in the main text.

II. SELF-CONSISTENT BORN APPROXIMATION

Here we follow the disorder Hamiltonian $H = \sum_{\mathbf{k}} c_{\mathbf{k}}^{\dagger} H_0(\mathbf{k}) c_{\mathbf{k}} + \int d\mathbf{r} U(\mathbf{r}) c_{\mathbf{r}}^{\dagger} \Lambda c_{\mathbf{r}}$, presented in the main text. To recapitulate, $c^{\dagger} \equiv (d^{\dagger}, f^{\dagger})$ is the electron creation operator for the two orbitals. $U(\mathbf{r})$ is the impurity potential, which is assumed to be short-ranged and characterized by $\langle U(\mathbf{r})U(\mathbf{r}') \rangle = U_0 \delta(\mathbf{r} - \mathbf{r}')$ under disorder average $\langle \dots \rangle$. Λ is the electron-impurity scattering vertex of the form $\Lambda = \alpha I + \beta \sigma_z$.

A. Conditions for Diagonal Self-energy

Since we are interested in the diagonal self-energy matrix Σ , we first briefly comment on the conditions for diagonal electron's self-energy Σ . There are two scenarios when solutions with diagonal Σ exist.

First scenario is the p -wave hybridization where $\Delta(\mathbf{k}) = -\Delta(-\mathbf{k})$. In this case, the self-consistent equation in self-consistent Born approximation (SCBA) is

$$\Sigma(\omega) = U_0^2 \int \frac{d^2\mathbf{k}}{(2\pi)^2} \Lambda(\omega - H_0 - \Sigma(\omega))^{-1} \Lambda \quad (6)$$

$$= U_0^2 \int \frac{d^2\mathbf{k}}{(2\pi)^2} \frac{1}{z_1 z_2 - \Delta^2(\mathbf{k})} \begin{pmatrix} (\alpha + \beta)^2 z_2 & (\alpha^2 - \beta^2) \Delta(\mathbf{k}) \\ (\alpha^2 - \beta^2) \Delta(\mathbf{k}) & (\alpha + \beta)^2 z_1 \end{pmatrix}, \quad (7)$$

where

$$z_1 = \omega - \Sigma_1 - \frac{k^2}{2m_1} - \frac{g}{2}, \quad z_2 = \omega - \Sigma_2 + \frac{k^2}{2m_2} + \frac{g}{2}, \quad (8)$$

are both functions even in \mathbf{k} . The odd function nature of $\Delta(\mathbf{k})$ guarantees the off-diagonal term in Σ to vanish after the integration.

Another scenario is the “incoherent” s -wave hybridization $\Delta(\mathbf{k}) = \Delta(-\mathbf{k})$, where there are two different impurity potentials U_1 and U_2 that scatter incoherently with two orbitals. It is based on the observation that if the impurity potential is only on one orbital, i.e., $\Lambda = (I \pm \sigma_z)/2$ or $\alpha = \beta$, the off-diagonal term in Σ will not be generated even for s -wave hybridization (Eq. (7)). To be more concrete, let

$$U(\mathbf{r})\Lambda = \begin{pmatrix} U_1(\mathbf{r}) & 0 \\ 0 & U_2(\mathbf{r}) \end{pmatrix}, \quad (9)$$

with $\langle U_i(\mathbf{r})U_i(\mathbf{r}') \rangle_j = U_i \delta(\mathbf{r} - \mathbf{r}') \delta_{ij}$, and $\langle U_1(\mathbf{r})U_2(\mathbf{r}') \rangle_i = 0$ for $i, j = 1, 2$. Here $\langle \cdot \cdot \cdot \rangle_i$ is the disorder average under impurity potential i . In this case, the SCBA equation becomes

$$\Sigma(\omega) = U_1^2 \int \frac{d^2\mathbf{k}}{(2\pi)^2} \Lambda_1(\omega - H_0 - \Sigma(\omega))^{-1} \Lambda_1 + U_2^2 \int \frac{d^2\mathbf{k}}{(2\pi)^2} \Lambda_2(\omega - H_0 - \Sigma(\omega))^{-1} \Lambda_2, \quad (10)$$

where $\Lambda_{1,2} = (I \pm \sigma_z)/2$. It is easy to verify both integrals in Eq. (10) is proportional to $\Lambda_{1,2} = (I \pm \sigma_z)/2$ respectively, so that the resulting Σ is diagonal.

B. Numerical Solutions

The numerical solution to Eq. (7) for p -wave hybridization $\Delta(\mathbf{k}) = v(k_x - ik_y)$ is shown in Fig. 1. The solution to “incoherent” s -wave hybridization is quantitatively the same and will thus be omitted. For this continuum model in two dimensions, the integral in Eq. (7) diverges logarithmically. In order to obtain reasonable results, we take a large cutoff in momentum k_{\max} that is much larger than all momentum scales in the problem. We confirm all following results are qualitatively independent of the cutoff.

The self-energy Σ is decomposed as

$$\text{Re}\Sigma = \begin{pmatrix} \bar{\mu} + \frac{\bar{g}}{2} & 0 \\ 0 & \bar{\mu} - \frac{\bar{g}}{2} \end{pmatrix}, \quad \text{Im}\Sigma = \begin{pmatrix} \Gamma_1 & 0 \\ 0 & \Gamma_2 \end{pmatrix}, \quad (11)$$

where $\bar{\mu}$ and \bar{g} are the renormalization of the chemical potential and fundamental gap, and Γ_i is the scattering rate for band ϵ_i .

The normalization of the chemical potential and the fundamental gap is always nonzero for nonzero U_0 , and is weakly dependent on ω . Note that \bar{g} always tends to invert the band gap further, which is consistent with the theory of topological Anderson insulators [1].

The scattering rates of the two bands Γ_1 and Γ_2 are strictly zero for ω inside the gap and small U_0 . This is because for small impurity potential $U_0 \ll \delta(k_F)$, the conservation of energy cannot be satisfied in order for electrons in the noninteracting bands to be scattered into the gap. In other words, the mechanism that generates the in-gap quasiparticle is non-perturbative in the hybridization gap $\delta(k_F)$. For large enough scattering potential $U_0 \sim \delta(k_F)$, $\Gamma_1(\omega)$ and $\Gamma_2(\omega)$ can be treated as nonzero constants at low energy $|\omega| \lesssim \delta(k_F)$. This is the assumption for the calculations in the rest of this paper.

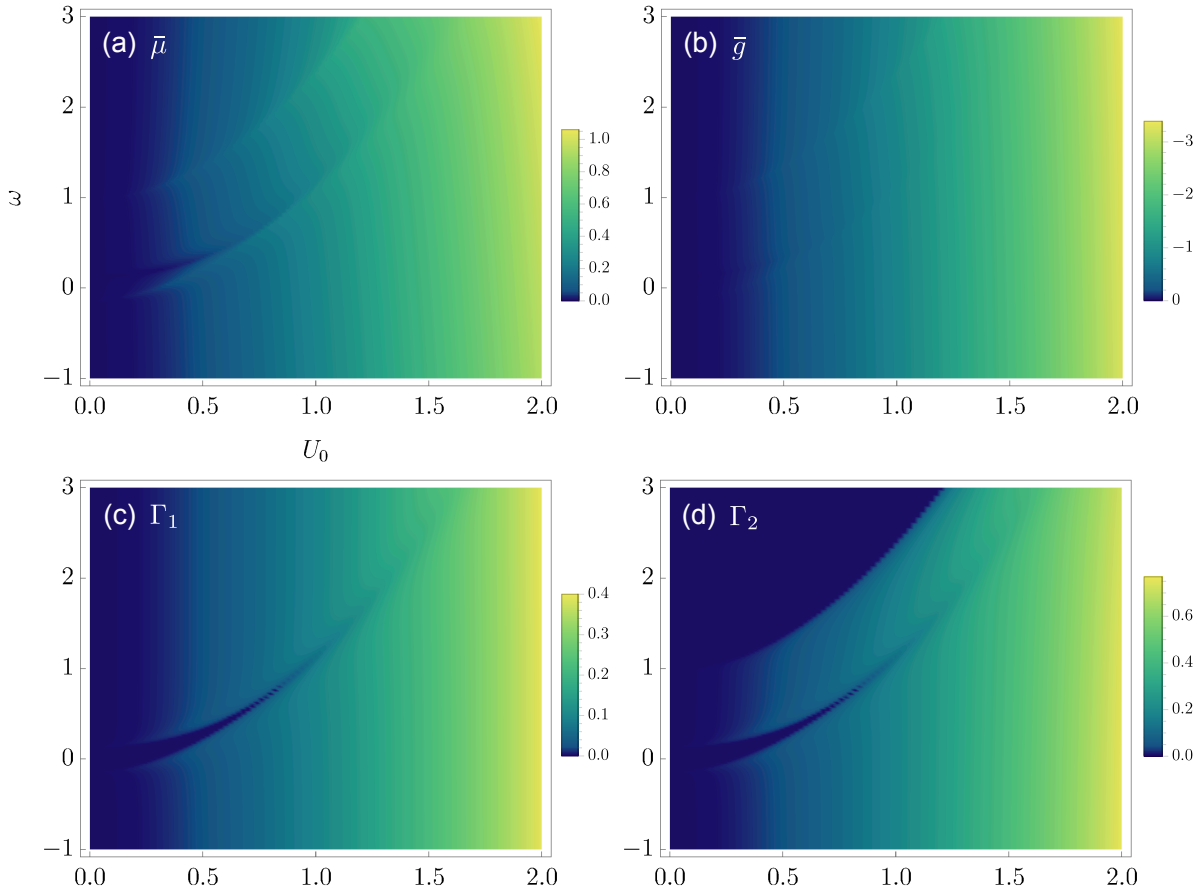


FIG. 1. Numerical solution of Eq. (7) with $m_2/m_1 = 50$ and $-\delta(k_F)/g = 0.02$. The impurity scattering vertex is $\Gamma = \alpha I + \beta \sigma_z$ with $\alpha = 0.6$ and $\beta = 0.4$. The cutoff is chosen so that $k_{\max} = 10^4 k_F$. All the energy units are $\delta(k_F)$.

III. MOMENTUM RESOLVED SPECTRAL FUNCTION AT ZERO FIELD

Here we analyze momentum resolved spectral functions $A(\mathbf{k}, \omega)$ in detail by comparing with the ARPES data from the experiment. We show that in order to capture some crucial features in the ARPES data, it is important to have $\gamma \neq 0$ or $\Gamma_1 \neq \Gamma_2$.

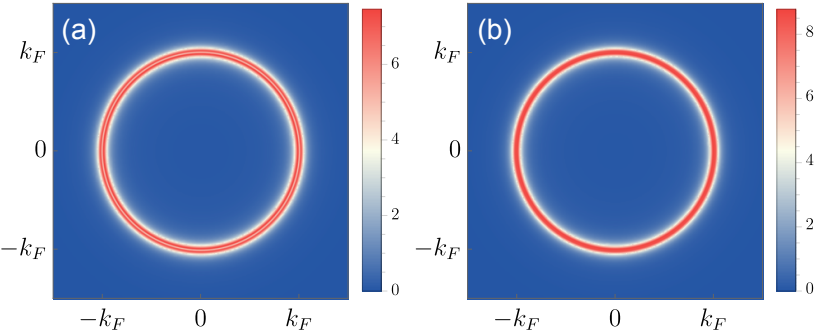


FIG. 2. $A(\mathbf{k}, E_F)$ as function of \mathbf{k} . Here $m_2/m_1 = 50$, $-\delta(k_F)/g = 0.01$ and $\Gamma_2/\delta(k_F) = 0.1$. (a) $\Gamma_1/\delta(k_F) = 0.7$; (b) $\Gamma_1/\delta(k_F) = 1.7$. The unit for $A(\mathbf{k}, E_F)$ is $1/\delta(k_F)$.

Following Fig. 2 in the main text, we first plot $A(\mathbf{k}, E_F)$ in momentum space. One can clearly see the Fermi surface of quasiparticles inside the hybridization gap. The two Fermi surfaces appeared in Fig. 2(a) are due to the indirect band gap of our model.

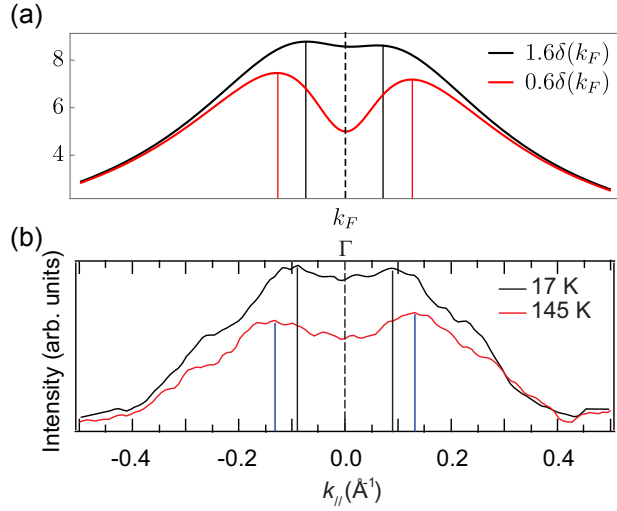


FIG. 3. (a) $A(k, E_F)$ as function of k for the same models in Fig. 2, with black line being $\gamma = 1.6\delta(k_F)$ ($\Gamma_2/\delta(k_F) = 1.6$, red line being $\gamma = 0.6\delta(k_F)$ ($\Gamma_2/\delta(k_F) = 0.7$). The unit for $A(k, E_F)$ is $1/\delta(k_F)$. (b) MDC ARPES result taken from FIG. 7(d) in Ref. [2].

To examine the momentum dependence more carefully, we plot $A(k, E_F)$ near $k = k_F$ in Fig. 3(a). This corresponds to the momentum distribution curve (MDC) in the ARPES data. With increasing $|\gamma|$, two features become evident: i) the spectral densities are more concentrated near the hybridzatin gap; ii) the two peaks of the spectral function become closer. We compare the actual MDC from the experiment in Fig. 3(b). There are indeed two peaks in the MDC data, which are consistent with the two Fermi surfaces in our model. More interestingly, the temperature dependence of the MDC data can be fit well by tuning γ . In this way, $|\gamma|$ increases with lowering the temperature.

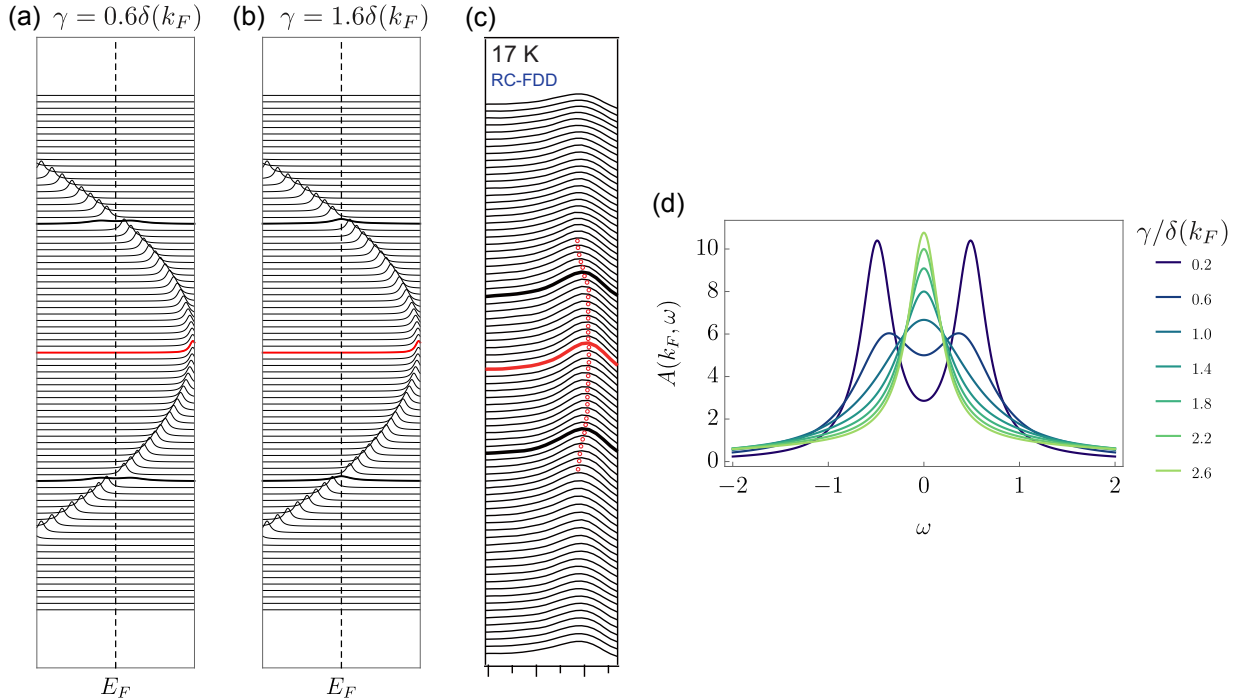


FIG. 4. (a)(b) $A(k, \omega)$ as function of both k and ω for the same models in Fig. 2. The red line represents $k = 0$ and the black lines represent $k = \pm k_F$. (c) EDC ARPES result taken from FIG. 7(b) in Ref. [2]. (d) $A(k_F, \omega)$ as function of ω for the same model in Fig. 2 but with different Γ_1 hence γ . The unit for spectral function is $1/\delta(k_F)$.

Finally, we plot $A(\mathbf{k}, \omega)$ as function of ω in both Fig. 4. This corresponds to the energy distribution curve (EDC) in the ARPES data. Here we focus on the feature at $k = k_F$. The positions of the peaks represent the real part of

the poles of the Green's function. When $|\gamma| \geq \delta(k_F)$, the two peaks merge into one at $\omega = E_F$, representing the vanishing of the hybridization gap and the disorder-induced metal. We compare the actual MDC from the experiment in Fig. 4(c). The single peak at $k = k_F$ suggests that $|\gamma| \gtrsim \delta(k_F)$, i.e., the system is in or at least very near the disorder-induced metal phase.

IV. LOW ENERGY DENSITY OF STATES AT ZERO FIELD

Consider the following quasiparticle Hamiltonian $H(k) = H_0(k) + \Sigma$ where $H_0(\mathbf{k})$ is given by Eq. (1) and Eq. (2) and Σ has constant diagonal imaginary part

$$\Sigma = \begin{pmatrix} -i\Gamma_1 & 0 \\ 0 & -i\Gamma_2 \end{pmatrix}. \quad (12)$$

By directly diagonalizing the matrix, we obtain the spectrum for the quasiparticle Hamiltonian:

$$\mathcal{E}_{\pm}(k) = \frac{1}{2} \left[\frac{k^2 - k_F^2}{2m_-} - i\Gamma \pm \sqrt{\left(\frac{k^2 - k_F^2}{2m_+} - i\gamma \right)^2 + \left(\frac{k\delta(k_F)}{k_F} \right)^2} \right], \quad (13)$$

where $\Gamma \equiv \Gamma_1 + \Gamma_2$, $\gamma \equiv \Gamma_1 - \Gamma_2$. Note the similarity between Eq. (3) and (13).

The corresponding spectral function is

$$A(\mathbf{k}, \omega) = -2\text{Im} \left(\frac{1}{\omega - \mathcal{E}_+(\mathbf{k})} + \frac{1}{\omega - \mathcal{E}_-(\mathbf{k})} \right) = -4\text{Im} \frac{\omega - \frac{1}{2} \left(\frac{k^2 - k_F^2}{2m_-} - i\Gamma \right)}{\left[\omega - \frac{1}{2} \left(\frac{k^2 - k_F^2}{2m_-} - i\Gamma \right) \right]^2 - \left(\frac{k^2 - k_F^2}{2m_+} - i\gamma \right)^2 - \left(\frac{k\delta(k_F)}{k_F} \right)^2}. \quad (14)$$

The density of states can be computed as the momentum integral of the spectral function:

$$A(\omega) = \int d\mathbf{k} A(\mathbf{k}, \omega) = \pi \int dk^2 A(k, \omega) \quad (15)$$

$$= -4\pi \text{Im} \int_0^{+\infty} dq \frac{\omega - \frac{1}{2} \left(\frac{q - k_F^2}{2m_-} - i\Gamma \right)}{\left[\omega - \frac{1}{2} \left(\frac{q - k_F^2}{2m_-} - i\Gamma \right) \right]^2 - \left(\frac{q - k_F^2}{2m_+} - i\gamma \right)^2 - q \left(\frac{\delta(k_F)}{k_F} \right)^2} \quad (16)$$

$$= -4\pi \text{Im} \int_0^{+\infty} dq \frac{aq + b}{q^2 + cq + d}, \quad (17)$$

$$= -4\pi \text{Im} \left[\frac{2b - ac}{\sqrt{4d - c^2}} \arctan \left(\frac{2q + c}{\sqrt{4d - c^2}} \right) + \frac{a}{2} \log(q^2 + cq + d) \right] \Big|_0^{+\infty}, \quad (18)$$

with

$$a \equiv -m_1 + m_2, \quad (19)$$

$$b \equiv k_F^2(m_1 - m_2) - 2m_1m_2(2\omega + i\Gamma), \quad (20)$$

$$c \equiv -2k_F^2 - 2m_1(\omega + i\Gamma_1) + 2m_2(\omega + i\Gamma_2) + m_1m_2\delta^2(k_F)/k_F^2, \quad (21)$$

$$d \equiv [k_F^2 + 2m_1(\omega + i\Gamma_1)] [k_F^2 - 2m_2(\omega + i\Gamma_2)]. \quad (22)$$

From Eq. (15) to (16) we have used the substitution $q = k^2$. Under the assumption of small hybridization gap $\delta(k_F) \ll k_F^2/\sqrt{m_1m_2}$, we can expand relevant expressions to the leading order of k_F :

$$2b - ac = -2(m_1 + m_2) [m_1(\omega + i\Gamma_1) + m_2(\omega + i\Gamma_2)], \quad (23)$$

$$4d - c^2 = 4m_1m_2\delta^2(k_F) - 4 [m_1(\omega + i\Gamma_1) + m_2(\omega + i\Gamma_2)]^2. \quad (24)$$

On the other hand,

$$\arctan \left(\frac{2q + c}{\sqrt{4d - c^2}} \right) \Big|_{q \rightarrow +\infty} = \frac{\pi}{2}, \quad \arctan \left(\frac{2q + c}{\sqrt{4d - c^2}} \right) \Big|_{q=0} = \arctan \left(\frac{c}{\sqrt{4d - c^2}} \right) = \arctan(-k_F^2) = -\frac{\pi}{2}, \quad (25)$$

$$\text{Im} \log(q^2 + cq + d) \Big|_{q \rightarrow +\infty} = 0, \quad \text{Im} \log(q^2 + cq + d) \Big|_{q=0} = \text{Im} \log(d) = \text{Im} \log(k_F^4) = 0. \quad (26)$$

Combine all these equations, we finally obtain

$$A(\omega) = 4\pi^2(m_1 + m_2)\text{Im} \left(\frac{m_1(\omega + i\Gamma_1) + m_2(\omega + i\Gamma_2)}{\sqrt{m_1m_2\delta^2(k_F) - [m_1(\omega + i\Gamma_1) + m_2(\omega + i\Gamma_2)]^2}} \right). \quad (27)$$

The density of states near the Fermi energy should be only dependent on the low energy properties of the model. It is important to notice that at two dimensions, the density of states of a quadratic band is just its effective mass:

$$A_i(\omega) = -2\pi\text{Im} \int_0^{+\infty} \frac{dq}{\omega - q/(2m_i) + i\eta} = 4\pi^2 m_i \theta(\omega). \quad (28)$$

Therefore, Equation (27) can be reexpressed as

$$A(\omega) = D_0 \text{Im} \frac{1}{\sqrt{\delta^2/(\omega + i\Gamma_A)^2 - 1}}, \quad (29)$$

where $D_0 = D_1 + D_2$, $D_i \equiv A_i(E_F)$ is the density of states at the Fermi energy in the absence of scattering and hybridization,

$$\delta = \frac{\sqrt{m_1m_2}}{m_1 + m_2} \delta(k_F), \quad \Gamma_A = \frac{m_1\Gamma_1 + m_2\Gamma_2}{m_1 + m_2}, \quad (30)$$

are the real band gap (as $\text{Im}\sqrt{\delta^2/\omega^2 - 1} = 0$ for $\omega^2 < \delta^2$), and the scattering rate weighted by the effective masses respectively. This is the Eq. (5) in the main text. Note that in this way we reproduce the band gap obtained in Eq. (5).

It is also instructive to express Eq. (30) using Fermi velocities $v_i \equiv \partial\epsilon_i/\partial k(k_F) = k_F/m_i$. In this way:

$$\delta = \frac{\sqrt{v_1v_2}}{v_1 + v_2} \delta(k_F), \quad \Gamma_A = \frac{v_2\Gamma_1 + v_1\Gamma_2}{v_1 + v_2}, \quad (31)$$

Equation (31) can also be derived directly from the generic two-band Hamiltonian Eq. (1) by expanding $\epsilon_i(k) = \epsilon_i(k_F) + v_i(k - k_F)$ and $\Delta(\mathbf{k}) = \delta(k_F)$.

V. LOW ENERGY DENSITY OF STATES UNDER MAGNETIC FIELD

A. Landau Level Spectrum

If out of plane magnetic field is applied, the energy bands become Landau levels. With Pierels substitution, $\mathbf{k} \rightarrow \mathbf{k} - \mathbf{A}$, where \mathbf{A} is the vector potential that satisfies $\nabla \times \mathbf{A} = \mathbf{B}$. Here we have already taken $e = c = 1$ for simplicity. After taking the symmetric gauge, we have the following identification of the operators:

$$k_x - ik_y = \sqrt{2B}\hat{a}, \quad k_x + ik_y = \sqrt{2B}\hat{a}^\dagger, \quad (32)$$

$$k_x^2 + k_y^2 = 2B \left(\hat{a}^\dagger \hat{a} + \frac{1}{2} \right). \quad (33)$$

where \hat{a}, \hat{a}^\dagger are lowering and raising operators for the quantum harmonic oscillator energy eigenstates: $\hat{a}|n\rangle = \sqrt{n}|n-1\rangle$ and $\hat{a}^\dagger|n\rangle = \sqrt{n+1}|n+1\rangle$. The noninteracting Hamiltonian then becomes

$$H_0 = \begin{pmatrix} \frac{B}{m_1} (\hat{a}^\dagger \hat{a} + \frac{1}{2}) + \frac{g}{2} + \mu_0 & \sqrt{2B}v\hat{a} \\ \sqrt{2B}v\hat{a}^\dagger & -\frac{B}{m_2} (\hat{a}^\dagger \hat{a} + \frac{1}{2}) - \frac{g}{2} + \mu_0 \end{pmatrix}. \quad (34)$$

For $n = 1$, we solve the quasiparticle Hamiltonian $H = H_0 + \Sigma$ with ansatz $(\psi_1, \psi_2) = (0, |0\rangle)$. The energy eigenvalue is

$$E_{n=0} = \mu_0 - \frac{g}{2} - i\Gamma_2 - \frac{B}{2m_2}, \quad (35)$$

which increases linearly with magnetic field, and does not contribute to the quantum oscillation.

For $n \geq 1$, we solve the quasiparticle Hamiltonian with ansatz $(\psi_1, \psi_2) = (c_1 |n-1\rangle, c_2 |n\rangle)$. The energy eigenvalues are

$$E_{n \geq 1, \pm} = \frac{1}{2} \left(\epsilon_{1,n} - \epsilon_{2,n} - i\Gamma \pm \sqrt{[(\epsilon_{1,n} + \epsilon_{2,n}) - i\gamma]^2 + v^2(8nB)} \right), \quad (36)$$

where

$$\epsilon_{1,n} = \frac{B}{m_1} \left(n - \frac{1}{2} \right) + \frac{g}{2} + \mu_0, \quad \epsilon_{2,n} = \frac{B}{m_2} \left(n + \frac{1}{2} \right) + \frac{g}{2} - \mu_0. \quad (37)$$

For large Landau level index $n \gg 1$, Eq. (13) becomes Eq. (36) by replacing $k \rightarrow \sqrt{2nB}$. This is the semi-classical regime of the Landau level spectrum.

Apart from the Landau level index n , the angular momentum is another good quantum number under the symmetric gauge. This leads to a $D = B/(2\pi)$ degeneracy for each Landau level per unit area of the system.

Finally, we remark the effect of electron spins. We have been focused on $\sigma_z s_z = -1$ sector of the full Hamiltonian. For the $\sigma_z s_z = 1$ sector, the Hamiltonian is H_0^T . The Landau level spectrum can be similarly obtained as

$$E_{n=0} = \mu_0 + \frac{g}{2} - i\Gamma_1 + \frac{B}{2m_1}, \quad (38)$$

and Eq. (36) with

$$\epsilon_{1,n} = \frac{B}{m_1} \left(n + \frac{1}{2} \right) + \frac{g}{2} + \mu_0, \quad \epsilon_{2,n} = \frac{B}{m_2} \left(n - \frac{1}{2} \right) + \frac{g}{2} - \mu_0. \quad (39)$$

Note that in the semi-classical regime, the Landau level spectra of both H^\uparrow and H^\downarrow are the same. Since in the following, we will carry out our calculation in this regime (weak magnetic field limit), it is safe to ignore the difference between H^\uparrow and H^\downarrow .

B. Low Energy Density of States

With magnetic field, the spectral function is computed by (neglecting lowest Landau level)

$$A(\omega) = -2D \text{Im} \sum_{n=1}^{\infty} \left(\frac{1}{\omega - E_{n,+}} + \frac{1}{\omega - E_{n,-}} \right), \quad (40)$$

where $D = B/(2\pi)$ is the degeneracy of the Landau level. This summation can be recast into an integral using Poisson summation formula: $A(\omega) = \sum_{k=0}^{\infty} A_k(\omega)$, where

$$A_k(\omega) = -4D \text{Im} \int_1^{\infty} dx \cos(2\pi kx) \left(\frac{1}{\omega - E_{x,+}} + \frac{1}{\omega - E_{x,-}} \right). \quad (41)$$

With the assumption of small hybridization gap $\delta(k_F) \ll k_F^2/\sqrt{m_1 m_2}$ and weak magnetic field $B \ll k_F^2$, the integrand can be simplified as

$$A_k(\omega) = \text{Im} \frac{-1}{\pi \sqrt{[(m_1 + m_2)\omega + i(m_1\Gamma_1 + m_2\Gamma_2)]^2 - m_1 m_2 \delta^2(k_F)}} \int_1^{+\infty} dx \cos(2\pi kx) \left(\frac{c_+}{x - x_+} - \frac{c_-}{x - x_-} \right), \quad (42)$$

$$c_{\pm} = (m_1 + m_2) [(m_1 + m_2)\omega + i(m_1\Gamma_1 + m_2\Gamma_2)] \pm (m_1 - m_2) \sqrt{[(m_1 + m_2)\omega + i(m_1\Gamma_1 + m_2\Gamma_2)]^2 - m_1 m_2 \delta^2(k_F)}, \quad (43)$$

$$x_{\pm} = \frac{k_F^2 + (m_1 - m_2)\omega + i(m_1\Gamma_1 - m_2\Gamma_2) \pm \sqrt{[(m_1 + m_2)\omega + i(m_1\Gamma_1 + m_2\Gamma_2)]^2 - m_1 m_2 \delta^2(k_F)}}{2B}. \quad (44)$$

Note that by assuming weak magnetic field, we are in fact in the semi-classical regime and the difference between H^\uparrow and H^\downarrow can be neglected.

Since we have already assumed weak magnetic field, the real parts of x_{\pm} are deep inside the right half of the complex plane. In this way, we can extend the integral range from $[1, +\infty)$ to $(-\infty, +\infty)$, so that the integral in Eq. (42) can be evaluated using residue theorem as long as it is not $\Gamma_1 = \Gamma_2 = 0$. Note the imaginary parts of x_+ and x_- are always of opposite signs, the integral contour (upper or lower plane) for x_+ and x_- are opposite. Denote $s \equiv \text{sgn Im } x_+ = \text{sgn } m_1$. The integral is evaluated as

$$\int_{-\infty}^{+\infty} dx \cos(2\pi kx) \left(\frac{c_+}{x - x_+} - \frac{c_-}{x - x_-} \right) = s\pi i (c_+ e^{2\pi iksx_+} + c_- e^{-2\pi iksx_-}). \quad (45)$$

Particularly inside the hybridization gap, the full form of the density of states is

$$A_k(\omega = 0) = -2 \cos\left(\frac{\pi k k_F^2}{B}\right) \sum_{i=\pm} M_i \exp(-\pi k \mathcal{D}_i), \quad (46)$$

with

$$M_{\pm} = \frac{s}{2} \left[\frac{(m_1 + m_2)(m_1 \Gamma_1 + m_2 \Gamma_2)}{\sqrt{(m_1 \Gamma_1 + m_2 \Gamma_2)^2 + m_1 m_2 \delta^2(k_F)}} \pm (m_1 - m_2) \right], \quad (47)$$

$$\mathcal{D}_{\pm} = \frac{s}{B} \left[\sqrt{(m_1 \Gamma_1 + m_2 \Gamma_2)^2 + m_1 m_2 \delta^2(k_F)} \pm (m_1 \Gamma_1 - m_2 \Gamma_2) \right], \quad (48)$$

being “effective masses” and Dingle exponents respectively. Note that the real part of x_{\pm} determines the oscillation period and the imaginary part determines the Dingle factor. c_{\pm} gives the “effective mass”. At zero hybridization gap limit $\delta(k_F) = 0$, the “effective masses” and the Dingle exponents become

$$M_+ = sm_1, M_- = sm_2, \quad (49)$$

$$\mathcal{D}_+ = 2sm_1\Gamma_1, \mathcal{D}_- = 2sm_2\Gamma_2, \quad (50)$$

which are exactly the effective masses and the Dingle exponents in normal metals.

It is instructive to rewrite Eq. (47) and (48) using $\Gamma_{A,D}$ and the indirect band gap δ :

$$M_{\pm} = \frac{s(m_1 + m_2)}{2} \left[\frac{1}{\sqrt{1 + \delta^2/\Gamma_A^2}} \pm \frac{m_1 - m_2}{m_1 + m_2} \right], \quad (51)$$

$$\mathcal{D}_{\pm} = \frac{s(m_1 + m_2)}{B} \left(\Gamma_A \sqrt{1 + \delta^2/\Gamma_A^2} \pm \Gamma_D \right), \quad (52)$$

where Γ_A and δ are defined in Eq. (30), and $\Gamma_D \equiv (m_1 \Gamma_1 + m_2 \Gamma_2)/(m_1 + m_2)$. These are Eq. (9) and (10) in the main text.

To further confirm that M_i is really the effective mass extracted from the temperature dependence of the oscillation amplitude, we explicitly compute the density of states at finite temperature, defined as

$$D(\omega, T) = - \int_{-\infty}^{+\infty} dE \frac{\partial n_F(E - \omega, T)}{\partial E} A(E) = \frac{1}{2T} \int_{-\infty}^{+\infty} \frac{dE}{1 + \cosh(\frac{E - \omega}{T})} A(E), \quad (53)$$

where $A(E)$ is the spectral function evaluated in Eq. (45). Here we have taken $k_B = 1$ for simplicity. Assume the temperature is small $T \ll \delta(k_F), B/m_{1,2}$, it suffices to expand $A(E)$ around $E = 0$, i.e., expand x_{\pm} to the leading order of ω and expand c_{\pm} to the zeroth order of ω :

$$x_{\pm} = x_{\pm,0} + \frac{\omega}{2B} \left[(m_1 - m_2) \pm \frac{(m_1 + m_2)(m_1 \Gamma_1 + m_2 \Gamma_2)}{\sqrt{(m_1 \Gamma_1 + m_2 \Gamma_2)^2 + m_1 m_2 \delta^2}}} \right], \quad (54)$$

where $x_{\pm,0}$ is Eq. (44) at $\omega = 0$. With the helpful of the Fourier transform

$$\int_{-\infty}^{\infty} dz \frac{e^{i\lambda z}}{1 + \cosh(bz)} = \frac{2\pi\lambda}{b^2} \frac{1}{\sinh(\pi\lambda/b)}, \quad (55)$$

the integral Eq. (53) can be performed analytically. The final result is

$$D_k(\omega = 0, T) = -2 \cos\left(\frac{\pi k k_F^2}{B}\right) \sum_{i=\pm} \frac{M_i \frac{2\pi^2 k T}{B/M_i}}{\sinh\left(\frac{2\pi^2 k T}{B/M_i}\right)} \exp(-\pi \mathcal{D}_i). \quad (56)$$

By doubling the density of states due to the contribution from $s = \uparrow$ spin sector, we get $D_1(\omega = 0, T)$ is Eq. (8) in the main text. The temperature dependence is exactly the Lifshitz-Kosevich factor for normal metals, with effective masses renormalized as Eq. (47).

[1] C. W. Groth, M. Wimmer, A. R. Akhmerov, J. Tworzydło, and C. W. J. Beenakker, “Theory of the Topological Anderson Insulator,” *Phys. Rev. Lett.* **103**, 196805 (2009).

[2] Q. Y. Chen, D. F. Xu, X. H. Niu, J. Jiang, R. Peng, H. C. Xu, C. H. P. Wen, Z. F. Ding, K. Huang, L. Shu, Y. J. Zhang, H. Lee, V. N. Strocov, M. Shi, F. Bisti, T. Schmitt, Y. B. Huang, P. Dudin, X. C. Lai, S. Kirchner, H. Q. Yuan, and D. L. Feng, “Direct observation of how the heavy-fermion state develops in CeCoIn₅,” *Phys. Rev. B* **96**, 045107 (2017).